Draft version October 14, 2021
Preprint typeset using LaTeX style emulateapj v. 5/25/10

THE SURFACE DENSITIES OF DISK BROWN DWARFS IN *JWST* SURVEYS

R. E. Ryan Jr.[1], I. N. Reid[1]

Draft version October 14, 2021

ABSTRACT

We present predictions for the surface density of ultracool dwarfs (with spectral types M8–T8) for a host of deep fields that are likely to be observed with the *James Webb Space Telescope*. Based on simple thin and thick/thin disk (exponential) models, we show the typical distance modulus is $\mu \approx 9.8$ mag, which at high Galactic latitude is $5 \log (2\, z_{scl}) - 5$. Since this is a property of the density distribution of an exponential disk, it is independent of spectral type or stellar sample. Using the published estimates of the ultracool dwarf luminosity function, we show that their number counts typically peak around $J \sim 24$ mag with a total surface density of $\Sigma \sim 0.3$ arcmin^{-2}, but with a strong dependence on galactic coordinate and spectral type. Owing to the exponential shape of the disk, the ultracool dwarfs are very rare at faint magnitudes ($J \geq 27$ mag), with typical densities of $\Sigma \sim 0.005$ arcmin^{-2} (or $\sim$20% of the total contribution within the field). Therefore in the very narrow and deep fields, we predict there are only a few ultracool dwarfs, and hence these stars are likely not a severe contaminant in searches for high-redshift galaxies. Furthermore the ultracool dwarfs are expected to be considerably brighter than the high-redshift galaxies, so samples near the faint-end of the high-redshift galaxy population will be the purest. We present the star-count formalism in a simplified way so that observers may easily predict the number of stars for their conditions (field, depth, wavelength, etc.).

Subject headings: Keywords: Galaxy: disk — Galaxy: structure — galaxies: high-redshift

1. INTRODUCTION

Number-magnitude counts have a long tradition of providing a simple, but effective tool for probing the distribution of stars within the Milky Way and the large-scale structure of the Universe (such as visual star-gaging of Herschel 1785). The application of photography to astronomical research in the late 1800s provided a means of obtaining permanent records of celestial objects, leading to systematic surveys such as the Plan of Areas (Kapteyn 1906) and the star-count analyses (Seares et al. 1925; Bok 1937). Additionally, photography also opened the way for surveys of the distribution of extragalactic nebulae, notably the Lick survey by Shane & Wirtanen (1954) and the Abell (1958) catalog of galaxy clusters, derived from the wide-field Schmidt plates of the first Palomar Observatory Sky Survey.

Photography captured images of the sky for posterity, but visual inspection of plates can only yield a qualitative understanding. The development of scanning densitometers in the 1970s provided the first means of quantifying photographic data for statistical analyses. When combined with deep imaging with 4-meter telescopes, photography yielded the first reliable color-magnitude diagrams for field stars and galaxies fainter than $\sim$ 20 mag (Kron 1980), and automated scans of wide-field Schmidt plate mapped the stellar distribution at bright magnitudes (e.g. Hewett, MacGillivray, & Dodd 1981; Gilmore, Reid, & Hewett 1985), but see Reid (1993a); Chincarini (2013) for a more extensive discussion of those developments. In more recent years, these investigations have given way to direct digital imaging, whether through narrow pencil-beam surveys, as exemplified by the Hubble Deep Field (HDF; Williams et al. 1996) and its successors, or through near all-sky surveys, such as the Sloan Digital Sky Survey (SDSS; York et al. 2000).

By and large, stars and galaxies occupy distinct domains in imaging surveys. At high galactic latitudes, stars are typically bright ($V \sim 20$ mag), while galaxies dominate at fainter magnitudes ($v \gtrsim 25$ mag). However rare objects often challenge conventional models and highlight short-comings in current theories. For example, Gilmore (1981) show that rare, faint stars can significantly contaminate samples of distant objects. In recent years, the focus has moved to significantly higher redshifts with the deepest surveys, aided partly by gravitational lensing, reaching beyond $z \sim 10$ (Coe et al. 2013; Ellis et al. 2013). At those redshifts, the Lyman break moves longwards of $\lambda \sim 1$ μm and galaxies have extremely red colors at near-infrared wavelengths. As Wilkins et al. (2014) have pointed out, very high-redshift galaxies and ultracool dwarfs often have similar near-infrared colors. In this paper, we consider the likely surface density of MLT-dwarfs (Kirkpatrick et al. 1999; Cushing et al. 2011) and their potential to bias studies of high-redshift galaxies.

This paper is organized as follows: In § 2 we give a brief discussion of stellar populations in the Milky Way, the relevant properties of ultracool dwarfs, and our choice of *representative* deep fields. In § 3 we detail the star-count formalism. In § 4 we discuss these results in the context of deep fields with the *Hubble Space Telescope* and the *James Webb Space Telescope*. Finally, in § 5 we conclude with a brief summary, reviewing the key points. Throughout this paper, we take care to explicitly state the magnitude system, to avoid confusion between Vega-based (often used in the Galactic and stellar community) and AB-based (the *de facto* standard in ex-

rryan@stsci.edu
[1] Space Telescope Science Institute, 3700 San Martin Dr., Baltimore, MD 21218

tragalactic work) magnitudes.

2. BACKGROUND

2.1. *The Stellar Populations of the Milky Way*

The resolved stellar constituents of nearby galaxies are generally categorized as members of distinct populations. Following Baade (1944) and Oort (1958), a *stellar population* is characterized as a collection of stars that have similar dynamical properties and share a common evolutionary scenario. Within the Milky Way, the main populations are the thin disk, the thick disk, the stellar halo, and the Galactic bulge/bar. The last-named population is generally confined within the central regions of the Galaxy (although radial migration may lead to some local representation), and we therefore focus the first two populations as representative of stars in the outer regions of the Galaxy in general and the Solar Neighborhood in particular. The main properties of these populations are well summarized by Freeman (2012).

Considering the three local populations, the thin disk is the dominant baryonic component, with a total mass of $\sim 5 \times 10^9$ $M_\odot$ and encompassing the gas and dust contributing the current star formation. The density distribution is generally well represented by a double-exponential, with a radial scale-length of $\sim 2.5-2.7$ kpc. Gas, dust, and young stars are closely confined to the Galactic midplane, with the vertical distribution increasing rapidly with age as the velocity increases due to scattering by massive objects such as molecular clouds (Spitzer & Schwarzschild 1951; Wielen 1977). The oldest stars in the disk have ages $\sim 8-10$ Gyr and distributed in a disk of scale-height of ~ 250 pc (Jurić et al. 2008).

The thick disk is a more extended component, again following a double-exponential distribution with a radial scale-length that is similar to the thin disk. Originally identified within the Galaxy from star count analyses by Gilmore & Reid (1983), the vertical distribution can be matched with a scale-height of $\sim 800-900$ pc. The color-magnitude diagram clearly indicates that this is an old population ($\sim 10-12$ Gyr), with essentially no on-going star formation. While the exact origin remains unclear, detailed spectroscopic analyses show that thick-disk stars have enhanced abundances of α-elements (Bensby 2013), indicating that the population formed rapidly, before type Ia supernovae could significantly enhance the iron abundance. The local density of thick-disk stars is $\sim 8-10\%$ that of the thin disk, with a likely total mass of $\sim (1-2) \times 10^9$ $M_\odot$.

2.2. *Colors of the Ultracool Dwarf Population*

Ultracool dwarfs have effective temperatures $T \lesssim 2500$ K and emergent spectra characterized by absorption from broad molecular and narrow resonance features (e.g. H_2O, FeH, TiO, CO, CH_4, Na I, and K I). Consequently these low-mass stars have very red optical/near-infrared broad-band colors, which are similar to galaxies at $z \gtrsim 6$ (Yan, Windhorst, & Cohen 2003; Ryan et al. 2005; Caballero, Burgasser, & Klement 2008; Wilkins et al. 2014). In Figure 1, we show the *JWST*/NIRCam broad-band colors synthesized from the IRTF/SpeX library[2]

[2] as compiled by A. Burgasser and available at http://pono.ucsd.edu/~adam/browndwarfs/spexprism/

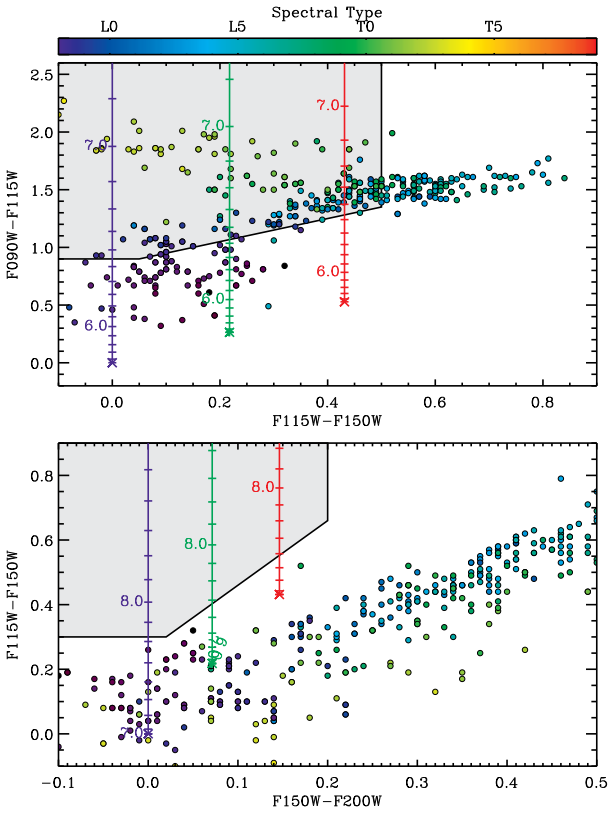

FIG. 1.— *JWST*/NIRCam broadband colors. Each point represents one object from the IRTF/SpeX library of A. Burgasser where the color encodes spectral type as indicated by the color bar. The colored tracks show the path of idealized, power-law spectra of the form $f_\lambda \propto \lambda^{-\beta}$ with $\beta =! -2$ (blue), $\beta = -1$ (green), and $\beta = 0$ (red), where each tick represents $\Delta z = 0.1$. The gray region shows a typical color-color region for selecting high-redshift galaxies ($z \gtrsim 6.5$), which demonstrates the well-known *identification degeneracy* widely discussed in the literature. While this degeneracy is readily broken with the suite of medium-bands designed to sample molecular absorption (from H_2O, CO, and CH_4) or additional broadbands at $\lambda \gtrsim 2$ μm, such data are rarely available. The stars (unlike the high-redshift galaxies) are not homogeneously distributed on the sky and so we provide simple models to predict the surface density of Galactic stars in § 3.

as colored points. The colored lines show the tracks of powerlaw spectra with $f_\lambda \propto \lambda^{-\beta}$ with blue ($\beta = 2$), green ($\beta = 1$), and red ($\beta = 0$). Additionally, we show an example selection region for $z \gtrsim 7$ galaxies as a gray polygon. With a limited number of broad-bands, the ultracool dwarfs and high-redshift galaxies have similar colors and are easily misidentified. Medium-bands tailored to sample the molecular features in the low-mass stars can easily break this *identification degeneracy*, but in their absence it is important to assess the potential number of stars in the sample.

2.3. *Stellar Luminosities*

We adopt the local J-band luminosity function pieced together from Cruz et al. (2007); Bochanski et al. (2010); Metchev et al. (2008), but a general calculation could transform to an arbitrary near-infrared passband using the IRTF/SpeX library. However these density estimates have modest uncertainties ($\delta\Phi/\Phi \sim 30\%$), so we take our luminosity function to be a fourth-order poly-

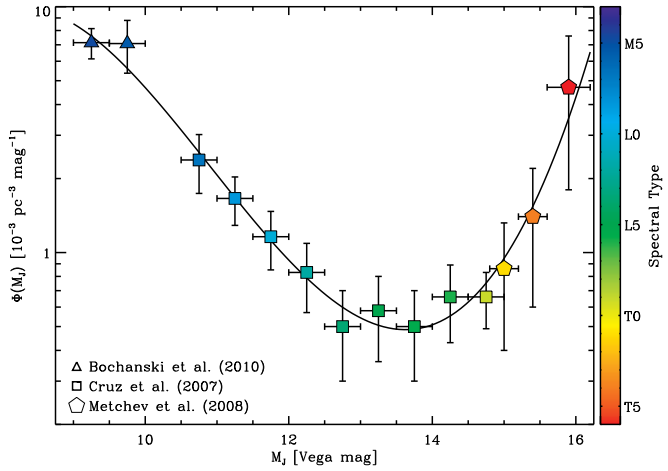

FIG. 2.— J(Vega)-band luminosity function. The symbols and colors represent the author from which the data are taken and the spectral type, respectively. The solid line shows the fourth-order fit given in equation (1). To map between luminosity and spectral type, we adopt the Hawley et al. (2002) relation. As mentioned in the text, we do not attempt to propagate the uncertainty on these data (or the uncertainty on the polynomial fit) into uncertainties on the observed number counts, as our primary goal is provide estimates for total number of brown dwarfs.

nomial fit for $8.5 \leq J \leq 16.5$ mag:

$$\begin{aligned}\log \Phi(J) = & -0.30 + 0.11\,(J-14) + 0.15\,(J-14)^2 \\ & + 0.015\,(J-14)^3 - 0.00020\,(J-14)^4\end{aligned} \quad (1)$$

where $\Phi(J)$ has units of 10^{-3} pc^{-3} mag^{-1} and J is Vega-based. In Figure 2, we show our polynomial luminosity function (solid line) and the observations as color symbols, where the color and shape represent spectral type and reference, respectively. As our primary goal is to predict the number counts at high-Galactic latitude, we do not propagate the uncertainty in these data or the corresponding polynomial model. Finally, we adopt the M_J(Vega)–spectral type relation of Hawley et al. (2002).

2.4. *Representative Deep Fields*

Although the precise details of the forthcoming *JWST* deep fields are not yet finalized, a reasonable strawman plan would use the broadband filters in the standard fields. We consider 11 fields, the five fields from the Cosmic Assembly Near-infrared Deep Extragalactic Legacy Survey (CANDELS; Koekemoer et al. 2011; Grogin et al. 2011) and the six Hubble Frontier Fields[3] (HFF; Lotz et al. in prep Lotz et al. 2014). In Table 1, we list the observational properties of these 11 fields, but regard COSMOS, Abell S1063, Abell 2744, and MACS J0717 as *representative* fields, since they cover a range of celestial coordinates and give the largest spread in the following predictions.

3. MODELING *PENCIL-BEAM* SURVEYS

The majority of recent surveys for high-redshift galaxies are based on deep, narrow-angle imaging observations. The number of stars N within such fields is given by integrating their density distribution $p(\mathbf{r}, M)$ over the sampled volume. Here we make the usual assumption that the stellar luminosity function $\phi(M)$ is independent of spatial distribution $n(\mathbf{r})$ or position in the Galaxy (Bahcall 1986); hence

$$p(\mathbf{r}, M)\,\mathrm{d}^3\mathbf{r}\,\mathrm{d}M = n(\mathbf{r})\,\phi(M)\,\mathrm{d}^3\mathbf{r}\,\mathrm{d}M, \quad (2)$$

but we recognize that the cooling of the brown dwarfs may lead to a vertical dependence on the luminosity function (Burgasser 2004; Ryan et al. 2011). We take $n(\mathbf{r})\,\mathrm{d}^3\mathbf{r}$ and $\phi(M)\,\mathrm{d}M$ to be dimensionless, and adopt the local luminosity function (as discussed in § 2.3). Therefore we must renormalize these distributions as:

$$n(\mathbf{r}_\odot) = \int \Phi(M')\,\mathrm{d}M' \equiv n_\odot, \quad (3)$$

where $\Phi(M)$ is the local luminosity function in units of pc^{-3} mag^{-1}. We renormalize the luminosity function as $\phi(M)\,\mathrm{d}M = n_\odot^{-1}\,\Phi(M)\,\mathrm{d}M$ to have units of mag^{-1}.

For this work, we consider only disk distributions, as the Galactic halo is at least 11 Gyr old (Kalirai 2012) and any brown dwarfs here would have cooled below our spectral-type range, but discuss the contribution in § 4. Assuming the standard double-exponential model, we have

$$\tilde{n}(r, z; r_s, z_s) = n_\odot\,\exp\left(\frac{r_\odot - r}{r_s} + \frac{|z_\odot| - |z|}{z_s}\right), \quad (4)$$

where $(r_\odot, z_\odot)$ represent the Solar position in the Galaxy. So, for a thick and thin disk the total density is given by:

$$n(r, z) = \tilde{n}(r, z; r_s, z_s) + f_t\,\tilde{n}(r, z; R_s, Z_s) \quad (5)$$

where f_t is the fraction of thick disk stars. The conversion from these cylindrical coordinates, assuming azimuthal symmetry based on the Galactic center, to spherical coordinates with to the Sun is given by Jurić et al. (2008):

$$r = \sqrt{r_0^2 + R^2\cos^2 b - 2Rr_0\cos b\cos\ell} \quad (6)$$

$$z = R\sin b + z_0, \quad (7)$$

where R is the heliocentric distance and (ℓ, b) are the Galactic coordinates of the field. In Table 2 we list the published estimates for the parameters of these distributions that we will adopt. With a change of variables from heliocentric distance to distance modulus $\mu = 5\log R - 5$, the distance modulus distribution is given by

$$n(\mu, \ell, b)\,\mathrm{d}\mu = \Delta\Omega\,n(R, \ell, b)\,R^2\,\mathrm{d}R \quad (8)$$

where $\Delta\Omega$ is the field-of-view. In Figure 3 we show the distance modulus distributions for the four representative, high-latitude fields. The colors represent the thin disk (blue), thick disk (red), and total (black). For fields at very high latitude (such as Abell 2744), the typical distance for a star is $2\,z_{\rm scl}$, which is *independent* of the luminosity of the star and is generically true for any population confined to the Galactic disk (e.g. Green et al. 2014). We give the peak and average distance modulus for all 11 potential *JWST* deep fields in Table 3.

The predicted stellar number count is given by integrating equation (2), which is the so-called *fundamental*

[3] http://www.stsci.edu/hst/campaigns/frontier-fields/

TABLE 1
Representative *JWST* Fields

Name	α ($^{\rm h}$ $^{\rm m}$ $^{\rm s}$)	δ ($^\circ$ $'$ $''$)	ℓ (deg)	b (deg)	$E^{\dagger}_{B-V}$ (mag)
Abell 2744	00 14 21.2	−30 23 50.1	8.89757	−81.23860	0.012
UKIDSS UDS	02 17 37.5	−05 12 00.0	158.95220	−51.54158	0.020
Abell 370	02 39 52.9	−01 34 36.5	173.00410	−53.57030	0.028
HUDF/GOODS-S	03 32 29.5	−27 48 18.3	223.56903	−54.43162	0.007
MACS J0416–2403	04 16 08.9	−24 04 28.7	221.08660	−44.05440	0.036
MACS J0717+3745	07 17 34.0	+37 44 49.0	180.24429	+21.04515	0.068
COSMOS	10 00 27.9	+02 12 03.5	236.82544	+42.11648	0.016
MACS J1149+2223	11 49 36.3	+22 23 58.1	228.16350	+75.19849	0.020
HDFN/GOODS-N	12 36 54.9	+62 14 18.9	125.86574	+54.80702	0.011
EGS	14 19 18.0	+03 55 18.0	103.29148	+54.82531	0.028
Abell S1063	22 48 44.4	−44 31 48.5	349.48345	−59.93298	0.010

†Taken from the NASA Extragalactic Database based on Schlafly & Finkbeiner (2011).

TABLE 2
Galactic Model Parameters

name	variable	value	reference
Solar radius	$r_\odot$	8000 pc	Reid (1993b)
Solar height	$z_\odot$	25 pc	Jurić et al. (2008)
thin-disk scale length	r_{scl}	2500 pc	Jurić et al. (2008)
thin-disk scale height	z_{scl}	290 pc	Ryan et al. (2011)
thick-disk scale length	R_{scl}	3600 pc	Jurić et al. (2008)
thick-disk scale height	Z_{scl}	1000 pc	Jurić et al. (2008)
fraction of thick-disk	f	0.13	Jurić et al. (2008)

TABLE 3
Distance Modulus Results

Field	thin disk		thick disk	
	$\mu_{\rm peak}$ (mag)	$\mu_{\rm ave}$ (mag)	$\mu_{\rm peak}$ (mag)	$\mu_{\rm ave}$ (mag)
Abell 2744	8.88	8.30	11.62	11.04
UKIDSS UDS	9.15	8.58	11.62	11.04
Abell 370	9.13	8.53	11.57	10.99
HUDF/GOODS-S	9.13	8.55	11.63	11.05
MACS J0416–2403	9.41	8.83	11.82	11.24
MACS J0717+3745	10.47	9.88	12.55	11.96
COSMOS	9.52	8.94	11.96	11.37
MACS J1149+2223	8.86	8.26	11.47	10.88
HDFN/GOODS-N	9.11	8.56	11.69	11.08
EGS	9.22	8.62	11.79	11.19
Abell S1063	9.28	8.69	12.19	11.60

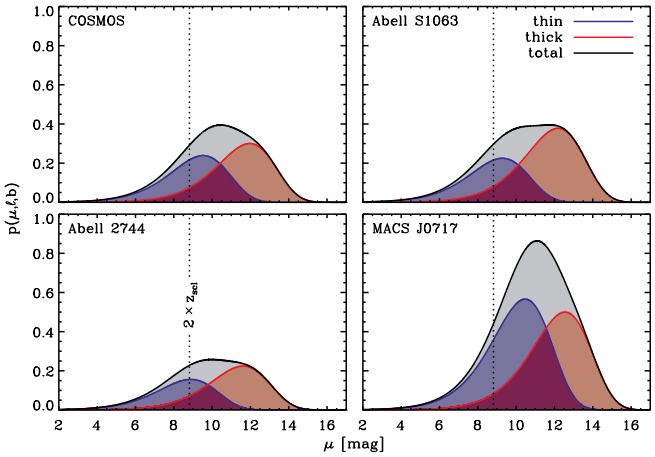

Fig. 3.— Distance distributions for representative fields. The blue, red, and gray distributions show the thin, thick, and total disk contributions. For fields pointed perpendicular to the Galactic plane, the distance modulus distribution from the thin disk will peak at $2\,z_{\rm scl}$, and the peak is only slightly more distant when including the thick disk. It is important to note, these distributions only depend on the Galactic model and not the luminosity of the stars in question. As such, these distributions are generically true and independent of bandpass, but are derived under the zero-extinction assumption. Including Galactic extinction is only necessary for low-latitude fields ($|b| \lesssim 10^\circ$, though there is a longitudinal dependence on this limit) and will introduce a wavelength dependence.

equation of stellar statistics (equation 1 of Bahcall 1986):

$$N(m,\ell,b)\,{\rm d}m = \Delta\Omega \int_0^\infty n(R,\ell,b)\,\phi(M)\,R^2\,{\rm d}R\,{\rm d}m, \quad (9)$$

where M is constrained to satisfy $M = m - \mu(R) - A(\ell,b,R)$, where $A(\cdot)$ is the extinction along a given line-of-sight as a function of distance. Since the typical *JWST* deep field is likely situated far from the Galactic plane, they will have low color excesses (typically $E_{B-V} \lesssim 0.03$ mag see Table 1; Schlafly & Finkbeiner 2011) and infrared extinctions of $A_{\rm IR} \lesssim 0.02$ mag (Schlegel, Finkbeiner, & Davis 1998). Moreover, since *JWST* will be able to detect L0 to $\sim$16 kpc and T8 to $\sim$3 kpc (assuming $J \sim 29$ mag and absolute magnitudes of Hawley et al. 2002), a full, three-dimensional description of $A(\cdot)$ is required for reliable number counts (Sale et al. 2009; Ryan et al. 2011; Green et al. 2014). Therefore we adopt $A(\ell,b,R) = 0$ mag, but stress that fields near the Galactic plane may require a more sophisticated treatment, which will modify our predictions. Using the definition from equation (8), we find that equation (9) is simply a convolution between the normalized luminosity function and the distance modulus distribution:

$$N(m,\ell,b)\,{\rm d}m = \Delta\Omega \int_{-\infty}^{+\infty} n(\mu,\ell,b)\,\phi(m-\mu)\,{\rm d}\mu\,{\rm d}m. \quad (10)$$

We show the differential (Figure 4) and integral (Figure 5) for our representative fields in units of arcmin^{-2}. As in Figure 3, the colors represent thin (blue), thick (red), and total (black) disk components. In the Appendix, we tabulate various statistics of the number counts for the 11 potential *JWST* deep fields broken down by spectral type (Tables 4–7). Since stars in the Milky Way are predominantly confined to an exponential

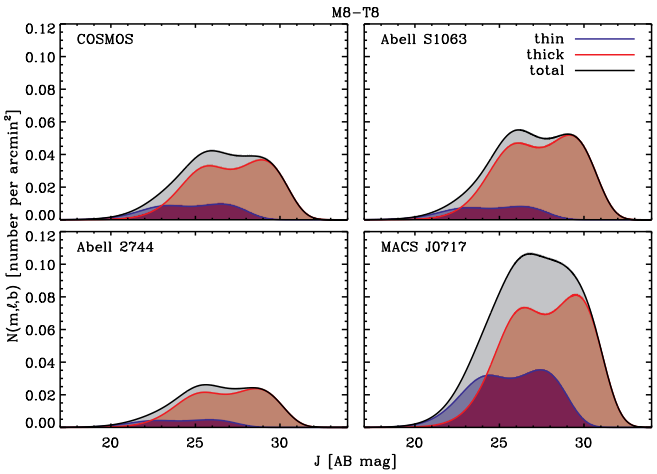

FIG. 4.— Differential number counts for representative *JWST* deep fields. Here we depict the contribution from the thin disk (blue), thick disk (red), and total disk populations (grey). The bimodal behavior comes from the two peaks in the extremal ranges of the luminosity function (see Figure 2). In the Appendix, we show similar plots for narrower ranges of spectral type.

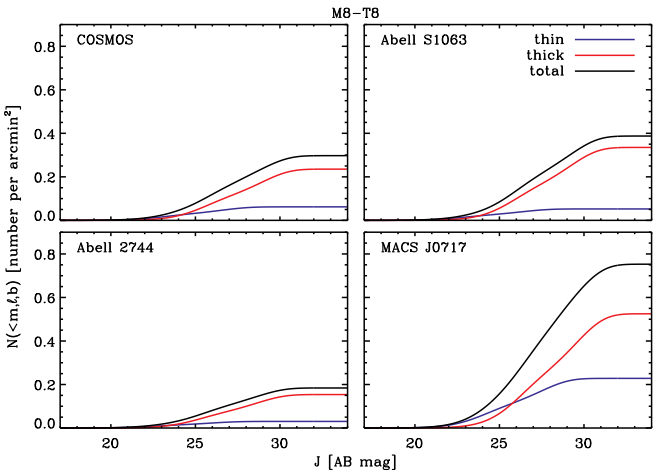

FIG. 5.— Integral number counts for representative *JWST* deep fields. The colors have the same meaning as in Figure 4.

disk, they are not generally not found at arbitrarily faint brightnesses. Although the ultracool dwarfs have very low-luminosities, they are expected to have $J \sim 24$ mag in high-latitude fields ($|b| \gtrsim 20°$).

4. DISCUSSION

We have demonstrated that for an idealized survey (ie. one with perfect sample completeness), the ultracool dwarfs are expected to be reasonably bright — reaching 50% of their totals near where their counts peak of $J \sim 24$ AB mag. However a realistic survey will not be so complete, and will therefore the expression in equation (9) should be modified to include a completeness function. In most cases, the completeness function does not have an explicit dependence on sky position, but rather is only modulated by the non-uniformity of the survey (Ryan et al. 2011; Holwerda et al. 2014). For most high-redshift galaxy surveys, the completeness is typically a weak function of brightness for AB $\lesssim 25$ mag (e.g. Bouwens et al. 2007), which leaves many of our results regarding the surface densities unchanged.

Thus far we have explicitly omitted a halo component, since the Galactic halo has an age of $\gtrsim 11$ Gyr (Kalirai 2012) — but here we illustrate its potential effect on our results. To have the colors consistent with a high-redshift galaxy, an ultracool dwarf would have a spectral type roughly L5–T5 (see Figure 1) and hence a temperature of $2000 - 1200$ K (Figure 7 of Kirkpatrick 2005). Based on the expected cooling curves (Burrows et al. 1997; Chabrier et al. 2000; Allard et al. 2001; Baraffe et al. 2003), a star with an age of 11.4 Gyr and temperature $1200 - 2000$ K would have a mass of $0.075 - 0.08\ M_\odot$ and likely sustain hydrogen fusion. Therefore we include a Galactic halo following the parameterization and values of Sesar, Jurić, & Ivezić (2011), but calculation over this narrow temperature range. The halo distribution peaks around $J \sim 30$ AB mag and increases the total surface density of ~ 0.1 arcmin^{-2}. This estimate depends strongly on the cooling models and star-formation history of brown dwarfs, and so should be regarded as preliminary. Nevertheless, *JWST* will have the ability to easily detect early-T dwarfs in the Galactic halo, indeed the existence of a sizable population veritably associated with the halo will be a useful boundary condition on the cooling models.

Throughout this work we have tacitly assumed that none of ultracool dwarfs are in unresolved binary systems. If we assume that equal-mass, unresolved binaries would have same colors, luminosities, and Galactic distribution as single stars, then the stars would be $2.5 \log 2 = 0.75$ mag too bright. If all stars were in binary pairs, then the number counts would shift ~ 0.75 mag to brighter limits, but the overall number of sources identified would remain constant (since the binaries are unresolved). Certainly this would exacerbate the issue of contamination, however this *maximum binarity* assumption is very conservative since the observed binary fractions are more like $\lesssim 25\%$ (e.g. Burgasser et al. 2007; Aberasturi et al. 2014). Moreover, Ryan et al. (2011) showed that the model number counts do not significantly change for binary fractions $\leq 40\%$.

5. SUMMARY

Since brown dwarfs have long been recognized as a potential contaminating source in high-redshift galaxy surveys (Yan, Windhorst, & Cohen 2003; Ryan et al. 2005; Caballero, Burgasser, & Klement 2008; Wilkins et al. 2014), we have provided tangible predictions for the surface density of these ultracool dwarfs using the best estimates for their luminosity function and Galactic distribution. We find that the highest surface densities are (not surprisingly) near the Galactic plane and with ~ 1 arcmin^{-2}. Therefore in existing datasets with *HST* the numbers are typically $\lesssim 1$ for a single WFC3 field-of-view (such as the HFF or HUDF) or ~ 40 for wide-field mosaics (such as CANDELS: UDS, EGS, or COSMOS). With *JWST* it will be possible to obtain many shallow fields (AB ~ 27) and search for dwarfs out to ~ 6 kpc, veritably sampling the Galactic halo. Although conclusively identifying a given dwarf as a member of the halo will require kinematic data, which will yield new constraints on the cooling models of ultracool dwarfs by providing robust samples of very old, but massive, objects.

The authors would like to thank Harry Ferguson for his thoughts regarding future deep fields with *JWST*. Support for this work was provided by NASA through grant number 13266 from the Space Telescope Science Institute, which is operated by AURA, Inc., under NASA contract NAS 5-26555. This research has benefited from the SpeX Prism Spectral Libraries, maintained by Adam Burgasser at http://pono.ucsd.edu/∼adam/browndwarfs/spexprism.

Facilities: JWST (NIRCam)

REFERENCES

Abell, G. O. 1958, ApJS, 3, 211
Aberasturi, M., Burgasser, A. J., Mora, A., Solano, E., Martín, E. L., Reid, I. N., & Looper, D. 2014, AJ, 148, 129
Allard, F., Hauschildt, P. H., Alexander, D. R., Tamanai, A., & Schweitzer A. 2001, ApJ, 556, 357
Baade, W. 1944, ApJ, 100, 137
Bahcall, J. N. 1986, ARA&A, 24, 577
Baraffe, I., Chabrier, G., Barman, T. S., Allard, F., & Hauschildt, P. H., 2003, A&A, 402, 701
Belokurov, V., Zucker, D. B., Evans, N. W., et al. 2006, ApJ, 642, L137
Bensby, T. 2013, IAU Symposium 298, (S. Feltzing, G. Zhao, N. Walton and P. Whitelock, eds)
Bochanski, J. J., Hawley, S. L., Covey, K. R., West, A. A., Reid, I. N., Golimowski, D. A., & Ivezić, Ž 2010, AJ, 139, 2679
Bok, B. J. 1937, Chicago: University of Chicago Press, 1937
Bouwens, R. J., Illingworth, G. D., Franx, M., & Ford, H. 2007, ApJ, 670, 928
Burgasser, A. J., 2004, ApJS, 155, 191
Burgasser, A. J., Reid, I. N., Siegler, N., Close, L., Allen, P., & Gizis, J. 2007, prpl conf. 427
Burrows, A., et al. 1997, ApJ, 491, 856
Caballero, J. A., Burgasser, A. J., & Klement, R. 2008, A&A, 488, 181
Chabrier, G., Baraffe, I., Allard F., & Hauschildt P. 2000, ApJ, 542, 464
Chincarini, G. 2013, arXiv:1305.2893
Coe, D., Zitrin, A., Carrasco, M., et al. 2013, ApJ, 762, 32
Cruz, K. L., et al. 2007, AJ, 133, 439
Cushing, M. C., et al. 2006, ApJ, 648, 614
Cushing, M. C., et al. 2011, ApJ, 743, 50
Ellis, R. S., McLure, R. J., Dunlop, J. S., et al. 2013, ApJ, 763, L7
Freeman, K. 2012, *Red Giants as Probes of the Structure and Evolution of the Milky Way*, 137
Gilmore, G. 1981, MNRAS, 195, 183
Gilmore, G., & Reid, N. 1983, MNRAS, 202, 1025
Gilmore, G., Reid, N., & Hewett, P. 1985, MNRAS, 213, 257
Green, G. M., et al. 2014, ApJ, 783, 114
Grogin, N. A., et al. 2011, ApJS, 197, 35
Hawley, S. L., et al. 2002, AJ, 123, 3409
Herschel, W. 1785, Royal Society of London Philosophical Transactions Series I, 75, 213
Hewett, P. C., MacGillivray, H. T., & Dodd, R. D. 1981, MNRAS, 195, 613
Holwerda, B. W., et al. 2014, ApJ, 788, 77
Jurić, M., Ivezić, Ž., Brooks, A., et al. 2008, ApJ, 673, 864
Kalirai, J. S. 2012, Natur, 486, 90
Kapteyn, J. C. 2006, The Plan of Selected Areas (Groningen University)
Kirkpatrick, J. D., Reid, I. N., Liebert, J., et al. 1999, ApJ, 519, 802
Kirkpatrick, J. D. 2005, ARA&A, 43, 195
Koekemoer, A. M., et al. 2011, ApJS, 197, 36
Kron, R. G. 1980, ApJS, 43, 305
Lotz, J., et al. 2014, AAS, #223, 254.01
Metchev, S. A., Kirkpatrick, J. D., Berriman, G. B., & Looper, D. 2008, ApJ, 676, 1281
Oort, J. H. 1958, Ricerche Astronomiche, 5, 415
Reid, N. 1993, Galaxy Evolution. The Milky Way Perspective, 49, 37
Reid, M. J. 1993, ARA&A, 31, 345
Ryan, R. E., Jr., Hathi, N. P., Cohen, S. H., & Windhorst, R. A. 2005, ApJ, 631, L159
Ryan, R. E., et al. 2011, ApJ, 739, 83
Sale, S. E., et al. 2009, MNRAS, 392, 497
Schlafly, E. F. & Finkbeiner, D. P. 2011, ApJ, 737, 103
Schlegel, D. J., Finkbeiner, D. P., & Davis, M. 1998, ApJ, 500, 525
Seares, F. H., van Rhijn, P. J., Joyner, M. C., & Richmond, M. L. 1925, ApJ, 62, 320
Sesar, B., Jurić, M., & Ivezić, Ž 2011, ApJ, 731, 4
Shane, C. D., & Wirtanen, C. A. 1954, AJ, 59, 285
Sommer-Larsen, J., & Zhen, C. 1990, MNRAS, 242, 10
Spitzer Jr., L. & Schwarzschild, M. 1951, ApJ, 114, 385
Stephens, D. C., et al. 2009, ApJ, 702, 154
Wielen, R. 1977, A&A, 60, 263
Williams, R. E. et al. 1996, AJ, 112, 1335
Wilkins, S. M., Stanway, E. R., & Bremer, M. N. 2014, MNRAS, accepted, arXiv: 1401.6822
Yan, H., Windhorst, R. A., & Cohen, S. H. 2003, ApJ, 585, L93
York, D. G., et al. 2000, AJ, 120, 1579

APPENDIX

RESULTS BY SPECTRAL TYPE

In the main text we presented differential and integral counts for all dwarfs near or below the hydrogen-burning limit, whose colors may be consistent with any high-redshift galaxy (ie. $z \gtrsim 6$ Yan, Windhorst, & Cohen 2003; Ryan et al. 2005; Caballero, Burgasser, & Klement 2008; Wilkins et al. 2014). However there are numerous methods for selection high-redshift samples (e.g. photometric redshifts, color/dropout selection, spectroscopic), which will undoubtedly have unique selection biases and purities. Therefore we have broken down the above results into four broad spectral classes M8-M9 (upper left), L0-L5 (upper right), L5-L9 (lower left), and T0-T5 (lower right) in Figures 6 and 7. As part of the online materials, we freely distribute J-band number counts for each field and spectral type.

TABLE 4
NUMBER COUNTS FOR M8–M9†

	thin disk					thick disk				
Field	$J_{\rm peak}$	$J_{1/2}$	$\Sigma_{<25}$	$\Sigma_{<27}$	Σ_{tot}	$J_{\rm peak}$	$J_{1/2}$	$\Sigma_{<25}$	$\Sigma_{<27}$	Σ_{tot}
Abell 2744	21.82	21.57	0.48	0.48	0.48	24.56	24.31	1.74	2.45	2.46
UKIDSS UDS	22.10	21.85	0.72	0.72	0.72	24.55	24.31	1.75	2.44	2.46
Abell 370	22.04	21.80	0.66	0.66	0.66	24.51	24.26	1.66	2.29	2.30
HUDF/GOODS-S	22.07	21.82	0.69	0.69	0.69	24.56	24.31	1.78	2.50	2.52
MACS J0416–2403	22.35	22.09	1.00	1.01	1.01	24.75	24.50	2.15	3.26	3.30
MACS J0717+3745	23.40	23.15	3.45	3.65	3.65	25.49	25.23	3.62	7.87	8.40
COSMOS	22.45	22.20	0.99	0.99	0.99	24.87	24.62	2.33	3.72	3.77
MACS J1149+2223	21.78	21.53	0.39	0.39	0.39	24.40	24.15	1.42	1.88	1.89
HDFN/GOODS-N	22.08	21.83	0.59	0.59	0.59	24.59	24.34	1.76	2.50	2.52
EGS	22.14	21.89	0.64	0.64	0.64	24.70	24.45	1.98	2.93	2.95
Abell S1063	22.22	21.97	0.84	0.84	0.84	25.12	24.87	2.89	5.22	5.36

†Columns 2–3 and 7–8 are in AB magnitudes while columns 4–6 and 9–11 are in 10^{-2} arcmin^{-2}

TABLE 5
NUMBER COUNTS FOR L0–L5†

	thin disk					thick disk				
Field	$J_{\rm peak}$	$J_{1/2}$	$\Sigma_{<25}$	$\Sigma_{<27}$	Σ_{tot}	$J_{\rm peak}$	$J_{1/2}$	$\Sigma_{<25}$	$\Sigma_{<27}$	Σ_{tot}
Abell 2744	22.62	22.39	0.62	0.63	0.63	25.36	25.13	1.47	2.99	3.19
UKIDSS UDS	22.91	22.68	0.91	0.93	0.93	25.36	25.13	1.47	2.99	3.18
Abell 370	22.85	22.62	0.84	0.86	0.86	25.31	25.08	1.41	2.81	2.97
HUDF/GOODS-S	22.87	22.64	0.87	0.89	0.89	25.37	25.14	1.50	3.06	3.26
MACS J0416–2403	23.15	22.92	1.25	1.30	1.30	25.56	25.33	1.73	3.91	4.27
MACS J0717+3745	24.21	23.98	3.72	4.71	4.72	26.29	26.06	2.54	8.35	10.87
COSMOS	23.26	23.03	1.22	1.28	1.28	25.67	25.44	1.83	4.39	4.88
MACS J1149+2223	22.58	22.36	0.50	0.50	0.50	25.20	24.98	1.24	2.34	2.45
HDFN/GOODS-N	22.88	22.66	0.75	0.76	0.76	25.40	25.17	1.47	3.05	3.26
EGS	22.94	22.71	0.80	0.83	0.83	25.50	25.27	1.61	3.54	3.82
Abell S1063	23.02	22.79	1.05	1.08	1.08	25.92	25.69	2.17	5.92	6.94

†Columns 2–3 and 7–8 are in AB magnitudes while columns 4–6 and 9–11 are in 10^{-2} arcmin^{-2}

TABLE 6
NUMBER COUNTS FOR L5–L9†

	thin disk					thick disk				
Field	$J_{\rm peak}$	$J_{1/2}$	$\Sigma_{<25}$	$\Sigma_{<27}$	Σ_{tot}	$J_{\rm peak}$	$J_{1/2}$	$\Sigma_{<25}$	$\Sigma_{<27}$	Σ_{tot}
Abell 2744	24.49	24.30	0.45	0.65	0.66	27.23	27.04	0.35	1.64	3.35
UKIDSS UDS	24.77	24.58	0.60	0.95	0.98	27.22	27.03	0.35	1.64	3.35
Abell 370	24.72	24.53	0.57	0.88	0.91	27.18	26.99	0.34	1.58	3.13
HUDF/GOODS-S	24.74	24.55	0.58	0.91	0.94	27.23	27.04	0.36	1.68	3.43
MACS J0416–2403	25.01	24.82	0.75	1.30	1.37	27.42	27.23	0.39	1.97	4.49
MACS J0717+3745	26.07	25.88	1.41	3.91	4.97	28.15	27.96	0.46	3.06	11.45
COSMOS	25.12	24.93	0.70	1.27	1.35	27.54	27.35	0.39	2.10	5.13
MACS J1149+2223	24.45	24.26	0.37	0.52	0.53	27.07	26.88	0.31	1.37	2.58
HDFN/GOODS-N	24.75	24.56	0.50	0.78	0.80	27.26	27.07	0.35	1.65	3.43
EGS	24.81	24.62	0.53	0.84	0.87	27.36	27.17	0.36	1.83	4.03
Abell S1063	24.88	24.69	0.67	1.10	1.14	27.79	27.60	0.43	2.54	7.31

†Columns 2–3 and 7–8 are in AB magnitudes while columns 4–6 and 9–11 are in 10^{-2} arcmin^{-2}

TABLE 7
NUMBER COUNTS FOR T0–T5†

Field	thin disk					thick disk				
	$J_{\rm peak}$	$J_{1/2}$	$\Sigma_{<25}$	$\Sigma_{<27}$	Σ_{tot}	$J_{\rm peak}$	$J_{1/2}$	$\Sigma_{<25}$	$\Sigma_{<27}$	Σ_{tot}
Abell 2744	25.99	25.75	0.15	0.44	0.52	28.74	28.49	0.05	0.41	2.63
UKIDSS UDS	26.28	26.03	0.18	0.60	0.77	28.73	28.49	0.05	0.41	2.63
Abell 370	26.22	25.98	0.17	0.57	0.71	28.69	28.44	0.05	0.40	2.46
HUDF/GOODS-S	26.25	26.00	0.18	0.58	0.74	28.74	28.49	0.05	0.41	2.69
MACS J0416–2403	26.52	26.27	0.20	0.77	1.08	28.93	28.68	0.05	0.45	3.53
MACS J0717+3745	27.58	27.34	0.26	1.57	3.91	29.66	29.42	0.05	0.54	8.99
COSMOS	26.63	26.38	0.18	0.73	1.06	29.05	28.80	0.05	0.46	4.03
MACS J1149+2223	25.96	25.71	0.13	0.36	0.41	28.58	28.33	0.04	0.36	2.02
HDFN/GOODS-N	26.26	26.01	0.15	0.50	0.63	28.77	28.52	0.04	0.40	2.69
EGS	26.32	26.07	0.16	0.53	0.68	28.88	28.63	0.05	0.42	3.16
Abell S1063	26.39	26.15	0.19	0.68	0.90	29.30	29.05	0.05	0.51	5.74

†Columns 2–3 and 7–8 are in AB magnitudes while columns 4–6 and 9–11 are in 10^{-2} arcmin^{-2}

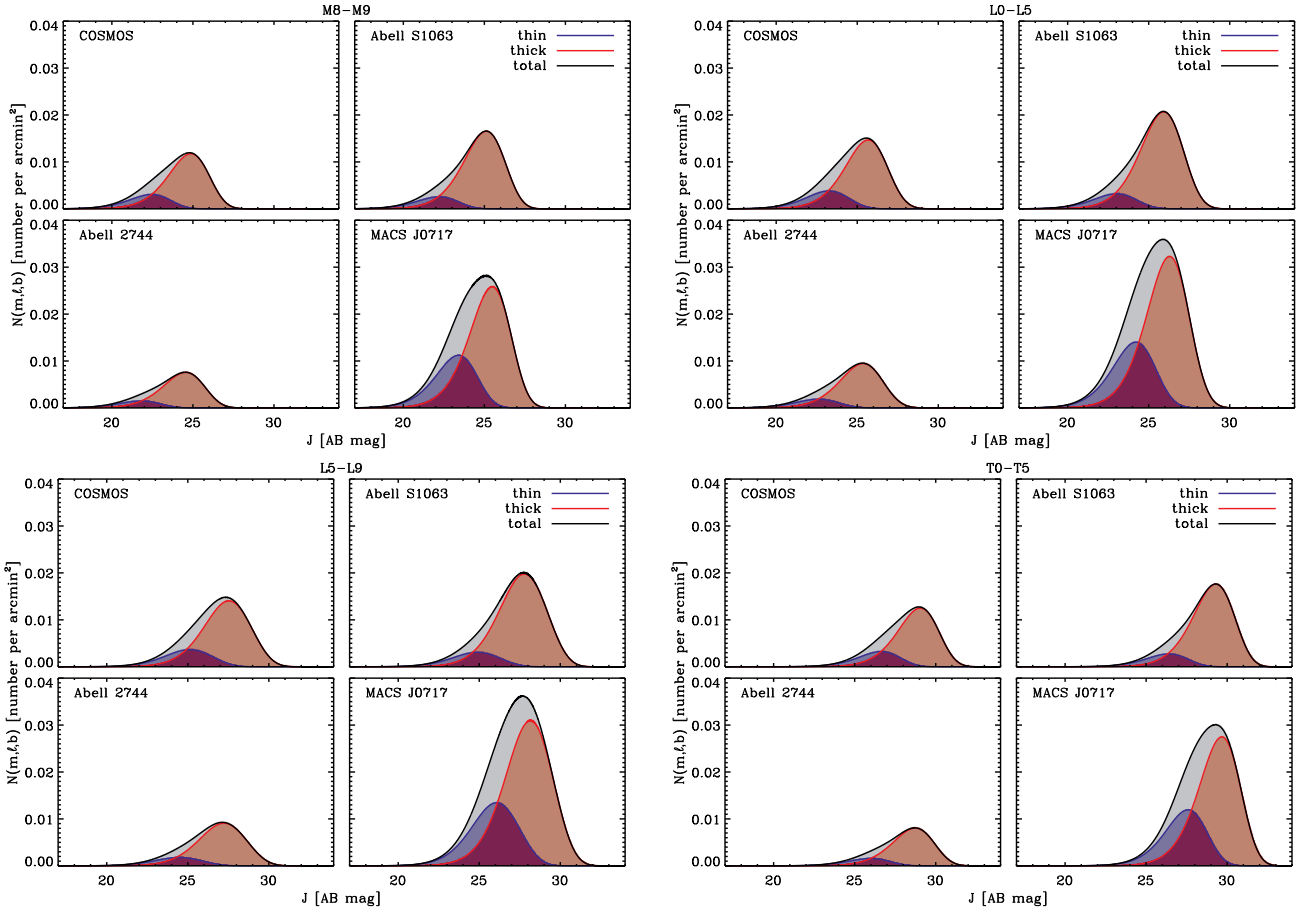

FIG. 6.— Differential counts for various spectral type ranges. Here the colors have the same meaning as Figure 4, but we show the differential counts of separate spectral types M8-M9 (upper left), L0-L5 (upper right), L5-L9 (lower left), and T0-T5 (lower right).

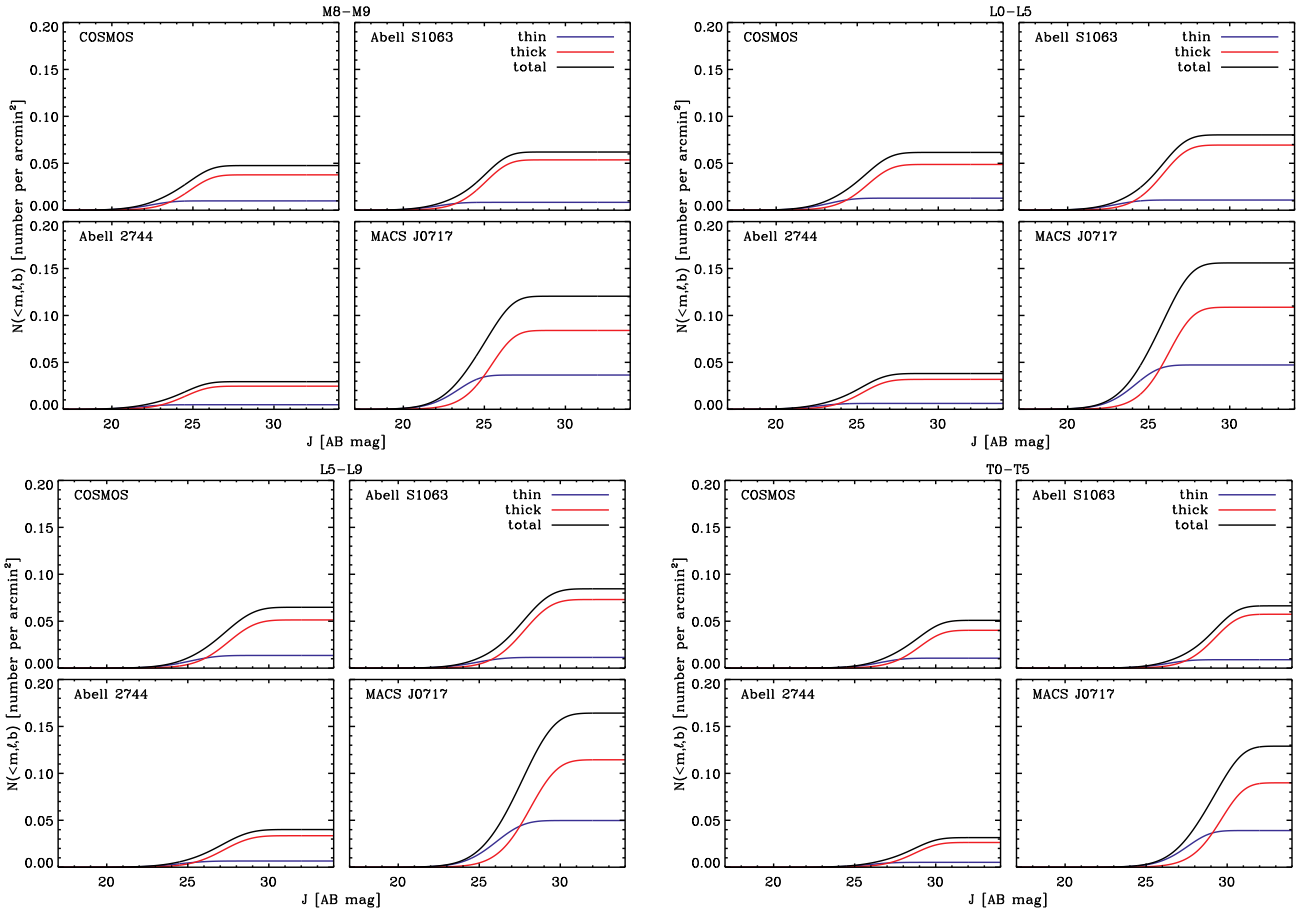

FIG. 7.— Cumulative counts for various spectral type ranges. Here the colors have the same meaning as Figure 5, but we show the differential counts of separate spectral types M8-M9 (upper left), L0-L5 (upper right), L5-L9 (lower left), and T0-T5 (lower right).